Journal Pre-proof

Anthocyanin-rich lingonberry extract improves intestinal homeostasis based on intestinal stem cells in high-fat-diet-fed mice *via* gut microbiota-mediated Wnt/PPAR signaling

Jiayi She, Xiaobin Hu, Jiannan Deng, Shuhang Fan, Qianyi Zhang, FuLi Nie, Jialei Zhang, Mark Christian, Zhenyu Wang, Xianjun Dai

PII: S2212-4292(24)01842-X

DOI: https://doi.org/10.1016/j.fbio.2024.105411

Reference: FBIO 105411

To appear in: *Food Bioscience*

Received Date: 5 August 2024

Revised Date: 29 October 2024

Accepted Date: 4 November 2024

Please cite this article as: She J., Hu X., Deng J., Fan S., Zhang Q., Nie F., Zhang J., Christian M., Wang Z. & Dai X., Anthocyanin-rich lingonberry extract improves intestinal homeostasis based on intestinal stem cells in high-fat-diet-fed mice *via* gut microbiota-mediated Wnt/PPAR signaling, *Food Bioscience*, https://doi.org/10.1016/j.fbio.2024.105411.

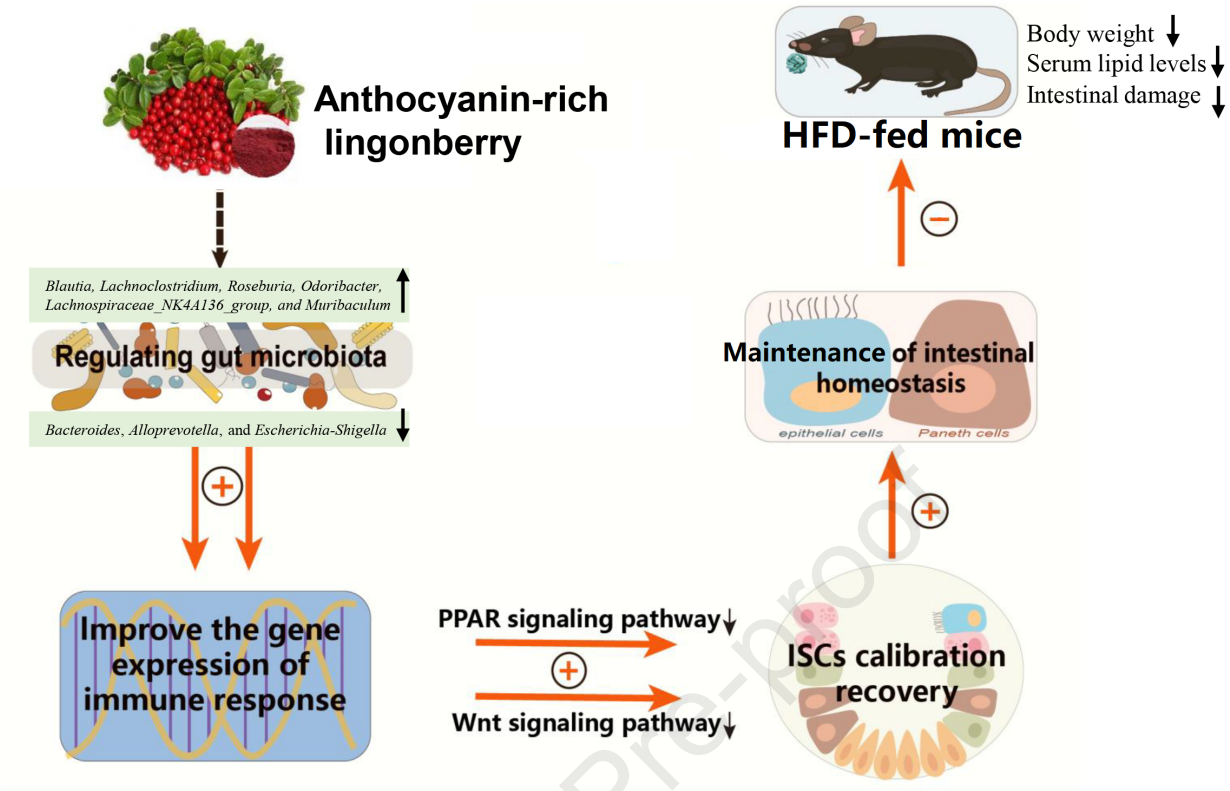

Anthocyanin-rich lingonberry extract improves intestinal homeostasis based on intestinal stem cells in high-fat-diet-fed mice *via* gut microbiota-mediated Wnt/PPAR signaling

Jiayi She[a,1], Xiaobin Hu[c,1], Jiannan Deng[a,1], Shuhang Fan[a], Qianyi Zhang[a], FuLi Nie[d], Jialei Zhang[d] , Mark Christian[e], Zhenyu Wang[*,a,b], & Xianjun Dai[*,a,b]

[a] College of Life Sciences, China Jiliang University, Hangzhou 310018, China.

[b] Key Laboratory of Specialty Agri-product Quality and Hazard Controlling Technology of Zhejiang Province, Hangzhou 310018, China.

[c] Xiangyang Hospital of Traditional Chinese Medicine, Xiangyang 441000, China.

[d] Huisong Pharmaceuticals Co., Ltd., 236 N Jianguo Road, Hangzhou 310003, China

[e] School of Science and Technology, Nottingham Trent University, Clifton, Nottingham, NG11 8NS, United Kingdom

[1] These authors contributed equally to this work.

Corresponding author: mrwangzyu@cjlu.edu.cn (Z. Wang), xjdai@cjlu.edu.cn (X. Dai)

Abstract

The Western diet impairs physiological health and leads to intestinal dysfunction. Lingonberries have the potential to ameliorate intestinal damage, although the underlying mechanisms are unclear. Here, the modulatory action of lingonberry anthocyanins on intestinal homeostasis in high-fat diet (HFD)-fed mice was investigated from the perspective of the intestinal flora-intestinal stem cells (ISCs) axis. The anthocyanin composition of lingonberry (*Vaccinium vitis-idaea* L.) extract was determined by high-performance liquid chromatography (HPLC). Anthocyanin-rich lingonberry extract (ARLE) was administered to HFD-fed mice for 9 weeks. Intestinal injury and ISCs fitness were analyzed by qPCR, immunofluorescence, and Western Blot. Moreover, the gut microbiota was analyzed by 16S rRNA sequencing and jejunum was used for RNA sequencing (RNA-Seq). The results showed that ARLE contained a total of 20 anthocyanins, which accounted for 36.0% of the extract. ARLE may balance intestinal homeostasis by enhancing the intestinal barrier and maintaining steady-state proliferation and differentiation of ISCs. RNA-seq revealed that ARLE supplementation improved the immune response and ISCs homeostasis by modulating Wnt/PPAR signaling, and this was potentially related to the gut microbiota. Our findings support that ARLE improved gut homeostasis and attenuated HFD-induced injury by regulating the gut microbiota-ISCs axis *via* Wnt/PPAR signaling.

Keywords: Anthocyanin-rich lingonberry extract; High-fat diet; Intestinal homeostasis; Microflora; Intestinal stem cells; Wnt/PPAR signaling

1. Introduction

Extensive epidemiological and preclinical investigations have established a strong association between long-term consumption of Western diets and the development of various diseases, including obesity, dyslipidemia, diabetes, nonalcoholic fatty liver disease, etc. (Su, et al., 2023). Moreover, the detrimental effects of a high-fat diet (HFD) may further impact emotions, cognition, and memory due to excessive free fatty acids (Amelianchik et al., 2022). Therefore, mitigating the adverse effects of a HFD is an important challenge to maintain health.

As the most important organ for digestion and absorption, the intestine is an important barrier against harmful foreign substances, which depends on the intestinal mucosal barrier. One of the potential risks of a HFD may be alterations in the intestinal epithelium, which can lead to dysfunction of intestinal homeostasis (Hooper et al., 2012). Intestinal stem cells (ISCs), which are located at the base of crypts, play a crucial role in maintaining intestinal equilibrium and epithelial tissue integrity by differentiating into diverse cell types within both the inner and outer layers of the intestine (Barker et al., 2007). A HFD is associated with detrimental effects on the fitness of ISCs through cell-autonomous or niche-dependent mechanisms (Murai & Matsuda, 2023). It was found that activation of lipid-sensing PPAR transcription factors by HFD can alter ISC function and their tumourigenic potential (Beyaz et al., 2021). Dysregulation of the Wnt signaling pathway caused by impaired bile acid secretion following HFD promotes the malignant transformation of ISCs (Fu et al., 2019). Furthermore, HFD downregulates the expression of the major histocompatibility

63 complex II gene in ISCs, thereby impairing interactions between the microbiome and
64 immune cells, which in turn promotes the development of intestinal tumours (Beyaz et
65 al., 2016). Therefore, the homeostasis of ISCs are pivotal factors responding to HFD-
66 induced stimulation and for mitigating its detrimental effects on health.

67 Anthocyanins are water-soluble flavonoids conferring colour to certain plants,
68 especially edible berries. They are usually bound to one or more glucose, galactose,
69 arabinose or rhamnose molecules *via* glycosidic bonds (Mattioli et al., 2020).
70 Lingonberry (*Vaccinium vitis-idaea* L.) is a small red berry of the genus *Vaccinium* and
71 termed a 'superfruit' due to containing the highest amount of antioxidants (e.g.,
72 vitamins, anthocyanins, and minerals) among berries (Yao et al., 2023). They exert
73 diverse physiological effects, including antioxidant, anti-obesity, anti-diabetic, anti-
74 inflammation, anti-tumor, and antimicrobial effects (Yao et al., 2023). Notably, they
75 also possess beneficial intestinal probiotic effects (Pärnänen et al., 2021). Evidence
76 suggests that lingonberry (especially 100 mg/kg) diminishes dextrose sodium sulfate
77 (DSS)-induced weight gain and ameliorates colon length shortening in mice. It also
78 downregulated the expression of cyclooxygenase-2 (COX-2), NF-κB, and iNOS in
79 colonic tissues, supporting the capacity of lingonberry to improve gut health (Jeon et
80 al., 2021). In addition, alteration of gut microbiota profiles may be an important
81 component of the positive actions of lingonberry to counteract the negative effects of
82 HFD on metabolic health (Marungruang et al., 2020). Research has shown that
83 lingonberry supplementation for 11 weeks could affect the expression of genes involved
84 in intestinal barrier function (decrease in expression of LPS-sensing Tlr4 and

macrophage marker Emr1, and increase in expression of the tight-junction protein occludin) and modify the composition and functionality of the gut microbiota (increase in *Akkermansia* and *Faecalibacterium*) in HFD-fed mice (Heyman-Lindén et al., 2016). Importantly, *in vitro* and *in vivo* experiments demonstrate that anthocyanins play a positive role against colorectal disease by altering the composition of the intestinal microbiota, protectively modulating the ISCs compartment, and suppressing inflammation and oxidative stress (Liu et al., 2024).

Based on the above evidence, it can be hypothesized that lingonberry anthocyanin can improve HFD-induced intestinal abnormalities through the communication between intestinal microbiota and ISCs. In this study, HFD-fed mice were used to explore the effect of anthocyanin-rich lingonberry extract (ARLE) on intestinal homeostasis based on the gut microbiota-ISCs axis. In addition, transcriptomics combined with Western blot analysis were applied to elucidate the mechanisms by which ARLE regulates ISCs homeostasis. Collectivelly, our results demonstrated the ability of lingonberry-based dietary manipulations to ameliorate the adverse effects of a high-calorie diet on intestinal homeostasis.

2. Materials and methods

2.1 Experimental reagents

Hematoxylin was purchased from Solarbio Science & Technology Co., Ltd. (Beijing, China); neutral gum, paraffin, and PBS were purchased from Biotechnology Co., Ltd. (Shanghai, China); alcohol, anhydrous ethanol, and xylene were purchased from Sinopharm Chemical Reagent Co., Ltd. (Shanghai, China). The following

antibodies, including anti-Ki67, anti-Lgr5, anti-MUC2, anti-SOX9, anti-c-Jun, anti-Rac1, anti-PPARd, anti-Wnt6, goat anti-rabbit IgG (H+L) Fluor 594-conjugated, and goat anti-rabbit IgG (H+L) FITC-conjugated, were shown in Table S2.

2.2 Analysis of anthocyanin in ARLE

The anthocyanin-rich lingonberry (*Vaccinium vitis-idaea* L.) extract (ARLE) was purchased from Huisong Pharmaceutical Co., Ltd (Hangzhou, China). The extract was obtained by 80% ethanol extraction, purification with YWD07 macroporous resin, concentration under reduced pressure and vacuum freeze-drying (Zhu et al., 2022). Then, a total of 125 mg of ARLE and anthocyanin standards were weighed, dissolved in a mixture of 2% hydrochloric acid and methanol (25 mL) , and filtered through a 0.45 μm membrane. Next, high-performance liquid chromatography (HPLC, Agilent, USA) with a photodiode array detector (PDA) was used to analyze the extract following the method of Deineka et al. (2020). The column used was a C_{18} column (4.6×250 mm, 5 μm, Agilent, USA). The sample size was 10 μL, the column temperature was 30 °C, and the flow rate was 1.0 mL/min. Mobile phase A was formic acid-water solution (8.5:91.5, v/v), and mobile phase B was formic acid-acetonitrile-methanol-water solution (8.5:22.5:22.5:41.5, v/v/v/v). The gradient program was: 0 min 93% (A), 0-35 min 75% (A), 35-45 min 65% (A), 45-50 min 100% (A), and kept at 100% (A) until 60 min. Quantification at a wavelength of 535 nm was performed by plotting HPLC peak areas against the concentrations (mg/g).

2.3 Animal experiment

Thirty 6-week-old male C57BL/6 mice (18±2 g) were purchased from Shanghai

Nanfang Mode Biotechnology Co., Ltd. (Shanghai, China) and housed with the approval with the Animal Care and Welfare Committee of China Jiliang University (No. CJLU2023004). All mice were raised in an animal facility with a temperature of 22 ± 1 °C, humidity of 50 ± 10%, and a 12-h light/dark cycle with free access to food and water. Control diets (CD, protein 20.54%, fat 12.79%, carbohydrate 66.67%) and HFD (protein 18.14%, fat 60.65%, carbohydrate 21.22%) were purchased from Jiangsu Coordinated Pharmaceutical Bioengineering Co., Ltd. (Jiangsu, China). All mice were acclimatized for one week and then divided into three groups (n=10) (Fig. 2A), namely, the CD group, HFD group, and HFD plus anthocyanin group (HFD-ARLE, 250 mg/kg). ARLE was dissolved in normal saline and administered by gavag for 9 weeks. The mouse weights were recorded every four days and food intake were calculated daily. At the end of the experiment, the mice were fasted for 12 h, and their weight and body length were measured to calculate the Lee's index.

2.4 Biochemical indexes analysis

After the mice were anesthetized with ethyl ether, blood was collected from the eyeballs and centrifuged at 3500 rpm (4 °C) for 15 min to obtain serum. The triglycerides (TG), total cholesterol (TC), low-density lipoprotein cholesterol (LDL-C), and high-density lipoprotein cholesterol (HDL-C) levels in serum were measured according to the Kit manufacturer's instructions (Nanjing Jiancheng Biotechnology Co., Ltd., Nanjing, China).

2.5 H&E staining

The jejunum and colon tissues were fixed in paraformaldehyde for 24 hours

followed by trimming and flattening. The tissues were dehydrated gradually as follows: 75% alcohol for 4 h, 85% alcohol for 2 h, 90% alcohol for 5 h, anhydrous ethanol for 30 min, benzyl alcohol for 5-10 min, xylene for 5-10 min, and placed in paraffin at 65 ℃ for 1 h. Before the paraffin solidified, the tissues were removed and placed into the embedding frame. After solidification, the paraffin blocks were removed and cut into 4 μm thick. The tissue sections were flattened in water at 40 °C and then lifted and dried in an oven at 60 °C. To prepare the H&E-stained samples, the sections from the hematoxylin solution were removed, washed with water, differentiated with 1% hydrochloric acid ethanol, washed with water for 5 min, stained with 0.6% ammonia, rinsed with water, and put into eosin staining solution for 1-3 min. Finally, the sections were sealed with neutral gum and observed under a microscope (Axio Scope.A1, Carl Zeiss, Germany).

2.6 PAS staining

To prepare the Periodic Acid-Schiff (PAS)-stained colon, Schiff reagent (Beyotime Co., Ltd., Shanghai, China) was added to the paraffin sections from the periodic acid solution at 37°C for 1 h. Then, the sections were rinsed with water, stained with hematoxylin for 30 s, washed twice with water for 3 min, and differentiated with hydrochloric acid and ethanol. Finally, the sections were washed, dehydrated, sealed with neutral gum and then observed and photographed for extensive evaluation using a microscope (Axio Scope.A1, Carl Zeiss, Germany).

2.7 Immunofluorescence staining

After the dehydrated jejunum sections were treated with antigen retrieval solution,

the sections were washed with PBS three times for 1 min each time and blocked with 5% goat serum (Beyotime Co., Ltd., Shanghai, China) at 37 °C for 30 min. Primary antibodies against Ki67 (1:400), Lgr5 (1:300), MUC2 (1:500), and SOX9 (1:300) were added to the blocked sections and incubated overnight at 4 °C. Sections were then reheated for 15 min and washed with TBST three times for 5 min. The sections were incubated with secondary antibodies (1:10,000) at room temperature for 1 h. After washing, DAPI (Beyotime Co., Ltd., Shanghai, China) was added to the sections, which were then incubated for 10 min at room temperature. Finally, the sections were treated with an anti-fluorescence quenching agent (Elabscience, E-IR-R119) and photographed under a fluorescence microscope (Axio Scope.A1, Carl Zeiss, Germany).

2.8 Immunohistochemical analysis

After antigen retrieval according to the above method, the jejunum sections were placed into 3% hydrogen peroxide, incubated at room temperature for 10 min, washed with PBS three times for 5 min each, and blocked with 5% goat serum for 10 min. The blocked sections were incubated overnight at 4 °C with anti-PCNA antibody (1:300) and washed with PBS three times for 5 min. The sections were incubated in a secondary antibody (1:20000) solution at room temperature for 30 min, followed by washing. The sections were then incubated with horseradish peroxidase labeling solution (Beyotime Co., Ltd., Shanghai, China) at 37 °C for 10 min, washed three times with PBS, stained with DAB chromogenic solution (Beyotime Co., Ltd., Shanghai, China), washed with water for 5 min, and counterstained with hematoxylin for 2 min. Finally, the sections were sealed with neutral gum to be observed and photographed for extensive evaluation

using a microscope (Axio Scope.A1, Carl Zeiss, Germany).

2.9 Western blot analysis

Jejunum tissues were lysed using the RIPA lysis buffer (P0013B, Beyotime), and supernatants were collected and subjected to electrophoresis. Then, the gel were blotted onto a PVDF membrane at 25 V constant voltage. The membrane was blocked with 5% skimmed milk for 1 h at room temperature and then incubated overnight at 4°C with primary antibodies, including anti-c-Jun (1:300), anti-Rac1 (1:500), anti-PPARδ (1:200) and anti-Wnt6 (1:200). The membrane was washed with TBST for three times (15 min), incubated with a secondary antibody (1:5000) solution at room temperature for 30 min. After washing three times with TBST, the membrane was incubated with ECL reagent and imaged using a gel imaging system (Bio-Rad Laboratories, CA, USA).

2.10 Gut microbiota analysis

Colonic contents were sent to Shanghai OE Biotech Co. Ltd. (Shanghai, China) and microbial DNA was extracted. The amplification and extraction of microbial DNA were performed according to the relevant parameters provided by Oebiotech Company. The results were analyzed by the OE Cloud Platform (https://cloud.oebiotech.cn). The detailed procedure was shown in the supplementary document.

2.11 RNA-seq analysis

Total RNA was extracted from jejunum using TRIzol reagent (Invitrogen, CA, USA) according to the manufacturer's protocol. RNA purity and concentration were evaluated using a NanoDrop 2000 spectrophotometer (Thermo Scientific, USA). RNA

integrity was assessed using an Agilent 2100 Bioanalyzer (Agilent Technologies, Santa Clara, CA, USA). The transcriptome sequencing and analysis were conducted by OE Biotech Co., Ltd. (Shanghai, China). The detailed procedure was shown in the supplementary document.

2.12 Statistical analysis

The data are expressed as the means±SEM. The statistical analyses were performed with GraphPad Prism 9.0 (GraphPad Software, San Diego, USA). One-way analysis of variance (ANOVA) with Tukey's multiple comparisons test was used for multiple comparisons. A T-test was performed to analyze the significant differences between two samples. * and ** indicate $P<0.05$ and $P<0.01$, respectively.

3. Results

3.1 Profile of anthocyanin in ARLE

As seen in Fig. 1, HPLC analysis showed ARLE was composed of twenty anthocyanins, constituting approximately 36.0% of the total extract. The amount and UV spectra of each anthocyanin are detailed in Table 1 and Table S1, respectively.

3.2 ARLE mitigates the negative physiological effects on HFD-fed mice

As shown in Fig. 2B, ARLE-treated mice exhibited lean body shape versus the mice in HFD group. In the 30th day, mice in the HFD-ARLE group had significantly lower body weights ($P<0.05$) compared to the HFD group (Fig. 2C), with a 30% reduction in body weight gain (Fig. 2D) ($P<0.01$). HFD feeding decreased food intake (Fig. 2E) ($P<0.01$) and increased energy intake (Fig. 2F) ($P<0.01$), whereas both food

and energy intake were further decreased after the ARLE intervention (P<0.01). Treatment with ARLE also induced a significant decrease in Lee's index (Fig. 2G) (P<0.05), and visceral white adipose tissue index (Fig. 2H) (P<0.05). Additionally, ARLE supplementation significantly reduced TG level (Fig. 2I) (P<0.01), increased HDL-C level (Fig. 2L), and decreased LDL-C level (Fig. 2K) (P<0.01), without a statistically significant effect on TC level (Fig. 2J). These findings suggest that dyslipidaemia in HFD-fed mice was significantly ameliorated by ARLE supplementation.

3.3 ARLE improves the intestinal homeostasis of HFD-fed mice

The length of the villi and the depth of the crypts in the jejunum are commonly used indicators for evaluating intestinal morphology. HFD can lead to a noticeable reduction in villus length and the shallowing of crypts, as confirmed by H&E staining (Fig. 3Aa-b). However, ARLE significantly restored or even increased the villus length (Fig. 3Ac and 3D) (P<0.01) and increased the crypt depth (Fig. 3E) (P<0.01). Additionally, H&E staining of the colonic tissue demonstrated that HFD induced structural abnormalities, resulting in a significant reduction in intestinal wall thickness (Fig. 3Bc), whereas ARLE supplementation restored colonic wall thickness to approach normal levels (Fig. 3F) (P<0.01). PAS staining showed a decrease in the PAS-positive area in the HFD group (Fig. 3Bd) compared with the CD group (Fig. 3Bb), which indicated a dramatically lower number of goblet cells within the colonic epithelium (Fig. 3G and 3H) (P<0.05). However, the administration of ARLE partially restored the structure of the colonic villi and crypts and replenished goblet cells, suggesting its improvement in

the colonic barrier function (Fig. 3Bf). In addition, immunofluorescence showed a significant increase in the staining intensity of MUC2 protein in the jejunum of ARLE-treated mice relative to the mice in HFD group (Fig. 3C and 3I) (P<0.05). qPCR and western blot analysis of MUC2 further supported this phenomenon (Fig. 3J, Fig. 3K, and Fig. S1) (P<0.05). Therefore, supplementation with ARLE ameliorated intestinal disorders in HFD-fed mice.

3.4 ARLE controls the malignant proliferation and differentiation of ISCs in HFD-fed mice

Immunohistochemistry analysis revealed that HFD significantly upregulated proliferating cell nuclear antigen (PCNA) in the jejunum crypts. However, ARLE effectively inhibited PCNA expression, suggesting its potential to alleviate HFD-induced ISCs abnormalities (Fig. 4A and 4E-F) (P<0.01). Furthermore, Lgr5, Ki67, and SOX9, which are indicators of ISC stemness and regenerative capacity, were examined in the different groups. Immunofluorescence staining and qPCR analysis showed significantly decreased expression of Ki67 (Fig. 4C and 4G-H), Lgr5 (Fig. 4B and 4I-J), and SOX9 (Fig. 4D and 4K-L) in the crypts of ARLE-treated mice. Correspondingly, western blot analysis demonstrated lower protein expression of Ki67 (Fig. 4M-N), Lgr5 (Fig. 4M and Fig. 4O), and SOX9 (Fig. 4M and 4P) in the jejunum crypts of ARLE-treated mice compared with the mice in the HFD group (P <0.05). The results above indicated that HFD-induced malignant proliferation of ISCs in the jejunum crypts could be significantly blunted by ARLE.

3.5 ARLE regulates the intestinal microflora of HFD-fed mice

Changes in the number of microbial species were observed between the HFD group and the HFD-ARLE group (Fig. 5A) (P<0.01), and the Shannon, ACE, and Chao1 indices showed a substantial increase in the microbial richness of ARLE-treated mice compared to those in the HFD group (Fig. 5B-D) (P<0.01). According to principal coordinate analysis (PCoA), the intestinal microbiota of mice in the HFD group was concentrated in the third quadrant, while the HFD-ARLE group was located in the first quadrant (Fig. 5F). Nonmetric multidimensional scaling (NMDS) analysis revealed similar results and an axisymmetric distribution was observed among the three groups (Fig. 5G). At the phylum level, ARLE treatment increased the Firmicutes/Bacteroidetes (F/B) ratio (Fig. 5E), which was attributed to a significant reduction in the abundance of family *Prevotellaceae* (a group of anaerobic bacteria in the phylum Bacteroidetes) (Fig. 5H). At the genus level (Fig. 5I), ARLE treatment significantly decreased the abundance of *Bacteroides* (Fig. 5K) (P<0.01), *Alloprevotella* (Fig. 5L) (P<0.05), and *Escherichia-Shigella* (Fig. 5M) (P<0.001), and significantly increased the abundance of *Blautia* (Fig. 5N) (P<0.01), *Lachnoclostridium* (Fig. 5O) (P<0.01), *Roseburia* (Fig. 5P) (P<0.01), *Odoribacter* (Fig. 5Q) (P<0.05), *Lachnospiraceae*_NK4A136_group (Fig. 5R) (P<0.01), and *Muribaculum* (Fig. 5S) (P<0.01).

3.6 ARLE manipulates the intestinal immune response of HFD-fed mice

According to principal component analysis (PCA) (Fig. 6A), RNA-seq showed that HFD had a significant effect on gene expression profiles in jejunum, with 657 genes downregulated and 435 genes upregulated (Fig. S2A). Compared to the HFD group, ARLE treatment induced 637 significantly upregulated genes and 353 significantly

downregulated genes (Fig. S2A). Additionally, volcano plot analysis highlighted 10 genes exhibiting substantial differential expression (Fig. 6B). Among these genes, *Defa39*, *Ang4*, *Mptx2*, *Defa31*, *Defa2*, *Defa32*, and *Defa33* were upregulated with ARLE supplementation. The differentially expressed genes were subjected to enrichment analysis using the GO (Fig. S2B), KEGG (Fig. S2C), Reactcome (Fig. S2D), and WikiPathways databases (Fig. S2E) for annotation. The GO analysis revealed that ARLE significantly change the innate immune response in the mucosa (NES<2.55, P<0.001, FDR<0.001) and the *Staphylococcus aureus* infection (NES<2.37, P<0.001, FDR<0.001) (Fig. 6C and 6E). In the ARLE group, genes of both pathways were significantly upregulated, mainly associated with *Defa* family genes (Fig. 6D and 6F). Integrated analysis of the microbiome and transcriptome (Fig. 6G) showed *Acetatifactor*, *Agathobacter*, *Lachnospiraceae_UCG-006*, *Bilophila*, and *the Eubacterium brachschy_ group* positively associated with *Mptx2* in the *Staphylococcus aureus* infection pathway and the *Defa* gene family in the intestine. Collectively, ARLE improved the expression of genes related to the immune response in the intestinal epithelium by regulating the gut microbiota.

3.7 ARLE affects the signaling pathways involved in ISCs homeostasis of HFD-fed mice

KEGG database annotation results demonstrated that ARLE induced significant alterations in the expression of genes involved in the Wnt and PPAR signaling pathways (Fig. S2C). Transcriptome GSEA showed that ARLE significantly affected changes in the PPAR (NES: −2.14, P<0.001, FDR: 0.004) and Wnt signaling pathways (NES: 1.61,

326 P<0.001, FDR: 0.006) (Fig. 7A and 7B). Moreover, ARLE downregulated the
327 expression of key genes in the Wnt and PPAR signaling pathways at the mRNA and
328 protein levels (Fig. 7C), namely, c-Jun (Fig. 7D and 7H) (P<0.01), Rac1 (Fig. 7E and
329 7I) (P<0.01), PPARd (Fig. 7F and 7J) (P<0.01), and Wnt6 (Fig. 7G and 7K) (P<0.01).

330 **4. Discussion**

331 Available evidence supports that the consumption of anthocyanin-rich foods, such
332 as berries, is linked to a reduction in the risk of obesity (Jamar et al., 2017). Earlier
333 studies carried out in HFD-fed mice found that medium (250 mg/kg) dose of
334 lingonberry extracts was more effective than low (125 mg/kg) and high (500 mg/kg)
335 doses in weight loss and blood lipid improvement, and didn't cause negative effects on
336 the kidneys as low and high doses did (Eid et al., 2014). In agreement with previous
337 studies (Eid et al., 2014; Kotowska et al., 2022; Ryyti et al., 2020; Ryyti et al., 2024),
338 our findings demonstrated that ARLE (250 mg/kg) supplementation significantly
339 inhibited weight gain, visceral white fat, and serum lipid levels in HFD-fed mice.
340 However, ARLE intervention did not affect serum TC level, potentially because
341 changes in cholesterol involve complex regulatory mechanisms related to the processes
342 of cholesterol uptake, synthesis, and excretion, and thus may not be significant in the
343 short term (Guo et al., 2024). In addition, a HFD usually increases cholesterol intake,
344 and ARLE may not be potent enough to counteract the elevating effects of HFD due to
345 insufficient dosage or duration. A HFD disrupts the equilibrium of intestinal
346 homeostasis by impairing the intestinal barrier and influencing immune cells (Dang et
347 al., 2023). Here, ARLE treatment partially restored both villus and crypt architecture in

the colon, as well as replenished monolayer columnar cells and goblet cells, which may be attributed to the improvement of intestinal function. Research has also shown that a long-term HFD induces proliferation of ISCs and promotes tumourigenesis in mice (Mana, et al., 2021). Evidence suggests that the PCNA, Lgr5, Ki67, and SOX9 proteins are strongly associated with aberrant ISCs proliferation and even intestinal cancer development (Kucera et al., 2018). Importantly, reduced expression of these markers in the HFD-ARLE group was found compared with the HFD group supporting the capacity of ARLE to protect against the malignant proliferation of ISCs and tumorigenicity. Therefore, ARLE can improve intestinal homeostasis in HFD-fed mice *via* regulating ISCs proliferation and differentiation in intestinal crypts (Li et al., 2020).

The intestine is a complex organ whose health is maintained through intricate interactions between nutrients, commensal microbiota and intestinal epithelium (Fang et al., 2023). The intestinal microbiota has been demonstrated to play important roles in intestinal homeostasis and the pathogenesis of metabolic diseases (Zhou et al., 2021). Supplementation of HFD-fed mice with lingonberries prevented increases in body weight, and metabolic and inflammatory parameters, which correlates with significant changes in microbiota composition (Heyman-Lindén et al., 2016). In Apoe knockout mice, lingonberries were found to decrease triglyceridemia, together with altered gut microbiota profiles (increase in *Bacteroides, Parabacteroides*, and *Clostridium*) (Matziouridou et al., 2016). Therefore, ARLE might modulate the composition and abundance of the gut microbiota to achieve its effects. Notably, alterations in the intestinal microbiota not only cause morphological changes in the

structure of intestinal villi and crypts, but also disrupt the cellular-level regulation of ISCs, leading to malignant proliferation (Xie et al., 2020), which induces the onset of intestinal cancers (Vernia et al., 2021). Here, ARLE supplementation significantly decreased the genus abundances of *Bacteroides*, *Alloprevotella*, and *Escherichia-Shigella* and increased the abundances of *Blautia*, *Lachnoclostridium*, *Lachnospiraceae*_NK4A136_group, *Roseburia*, *Odoribacter*, and *Muribaculum*. Previous studies have implicated *Escherichia-Shigella* (Li et al., 2022), *Bacteroides* (Zafar & Saier Jr, 2021), and *Alloprevotella* (Nguyen et al., 2022) as potential contributors to gut inflammation and disruption of the intestinal barrier. Conversely, an increase in other microorganisms, such as *Blautia* (Benítez-Páez et al., 2020), *Lachnospiraceae*_NK4A136_group (Yan et al., 2023), *Roseburia* (Zhao et al., 2022), *Odoribacter* (He et al., 2022), *Lachnoclostridium* (Wu et al., 2022), and *Muribaculum* (Huang et al., 2022) has been reported to produce short-chain fatty acids, which can reduce inflammation and affect intestinal homeostasis. As reported, *Lachnospiraceae* and *Blautia* are considered to play essential roles in promoting ISCs-mediated intestinal epithelial development and maintaining intestinal homeostasis in Wuliangye-treated mice (Zhu et al., 2024). Therefore, the modifications observed within intestinal microbial communities may serve as potential mechanisms underlying the role played by ARLE, which may affect the health status of HFD-fed mice.

Intestinal transcriptome analysis revealed that ARLE significantly increased the relative expression of genes related to the innate immune response in the mucosa and *Staphylococcus aureus* infection, and these genes were mostly members of a key *Defa*

392 gene family (Huang et al., 2022). The *Defa* gene family encodes al pha defensins and
393 plays a crucial role in various biological processes, including intestinal
394 iimmunomodulation, maintenance of mucosal barrier function, and regulation of
395 intestinal microbial homeostasis (Fu et al., 2023). Our results indicated that ARLE
396 could explicitly regulate the expression of *Defa* family genes, which can improve
397 intestinal homeostasis. Additionally, the expression of the *Mptx2* gene was elevated in
398 ARLE-treated mice, which could significantly decrease the risk of peritoneal infection
399 caused by exogenous methicillin-resistant *Staphylococcus aureus* (Zhu et al., 2022).
400 Combined analysis of the gut microbiome and jejunal transcriptomics revealed
401 significant associations between various microorganisms and the expression of the
402 *Mptx2* and *Defa* gene families. The above results further support that ARLE improved
403 immune function in the intestinal epithelium by regulating the gut microbiota.

404 Studies have implicated that microbiota can communicate with ISCs *via* Wnt or
405 PPAR signaling (Yao et al., 2023). Here, GSEA indicated that ARLE exerted regulatory
406 effects on the Wnt signaling and the PPAR signaling pathway. This is consistent with
407 a previous report that berries could inhibit the expression of markers (e.g., β-catenin,
408 Ki67) from the Wnt/β-catenin signaling pathway in colon adenocarcinoma cells (Slabá
409 et al., 2023). Notably, evidence has implicated the c-Jun gene in promoting intestinal
410 cancer (Nateri et al., 2005), and overexpression of Rac1 and Wnt6 proteins within the
411 Wnt pathway contributes to ISCs dyshomeostasis and colon tumorigenesis (Turdo et
412 al., 2020; Wang et al., 2021). Our findings demonstrated that ARLE significantly
413 suppressed the expression of the c-Jun, Rac1, and Wnt6 in the intestine, potentially

reducing the malignant proliferation of intestinal cells and early tumor development. Additionally, previous studies have reported a significant increase in the expression of PPARd target genes induced by HFD, which has been linked to tumor initiation in mouse intestines (Beyaz et al., 2016). In this study, ARLE treatment significantly decreased the mRNA and protein expression of PPARd. Collectively, these results suggested that ARLE had a regulatory role in ISCs proliferation through the Wnt/PPAR signaling. This is consistent with the beneficial effects of anthocyanins on intestinal health, including the regulation of intestinal microbiota and the promotion of intestinal barrier function (Liang et al., 2024).

Based on the above analysis, we propose a mechanism by which lingonberry anthocyanins protect against HFD-induced intestinal dyshomeostasis in association with alteration of the gut microbiota profile, increase in intestinal immune response, and the steady-state proliferation and differentiation of ISCs by regulating the Wnt and PPAR signaling.

5. Conclusion

In conclusion, ARLE could alleviate HFD-induced intestinal damage by improving intestinal immune function and controlling ISCs proliferation and differentiation. The homeostasis of ISCs could be regulated by remodeling gut microbiota *via* the Wnt/PPAR signaling pathway. The above results reveal the intricate relationships and mechanisms involving the ARLE-microbiome-ISCs axis, providing a theoretical basis for the development and utilization of lingonberry and anthocyanins in health food and foods for special medical purposes.

Conflicts of interest

No potential conflicts of interest were reported by the author(s).

Data availability

Data will be made available on request.

Acknowledgments

This research was funded by the Science and Technology Development Project in Zhejiang, China (2022C01030) and Project of Inovation and Entrepreneurship Training for National Undergraduates (202310356045). We thank all the authors for their invaluable comments on the manuscript.

References

Amelianchik, A., Sweetland-Martin, L., & Norris, E. H. (2022). The effect of dietary fat consumption on Alzheimer's disease pathogenesis in mouse models. *Translational Psychiatry, 2022, 12*(1), 293.

Barker, N., Van Es, J. H., Kuipers, J., Kujala, P., Van Den Born, M., Cozijnsen, M., et al. (2007). Identification of stem cells in small intestine and colon by marker gene Lgr5. *Nature*, *449*(7165), 1003-1007.

Benítez-Páez, A., Pugar, E. M. G. d., López-Almela, I., Moya-Pérez, Á., Codoñer-Franch, P., & Sanz, Y. (2020). Depletion of Blautia Species in the Microbiota of Obese Children Relates to Intestinal Inflammation and Metabolic Phenotype Worsening. *Msystems*, *5*(2): 10.

Beyaz, S., Chung, C., Mou, H., Bauer-Rowe, K. E., Xifaras, M. E., Ergin, I., et al. (2021). Dietary suppression of MHC class II expression in intestinal epithelial cells enhances intestinal tumorigenesis. *Cell Stem Cell*, *28*(11), 1922-1935.

Beyaz, S., Mana, M. D., Roper, J., Kedrin, D., Saadatpour, A., Hong, S.-J., et al. (2016). High-fat diet enhances stemness and tumorigenicity of intestinal progenitors. *Nature, 531*(7592), 53-58.

Dang, Y., Ma, C., Chen, K., Chen, Y., Jiang, M., Hu, K., et al. (2023). The Effects of a High-Fat Diet on Inflammatory Bowel Disease. *Biomolecules*, *13*(6), 905.

Deineka, V. I., Oleinits, E. Y., Kul'chenko, Y. Y., Blinova, I. P., & Deineka, L. A. (2020). Control of the Selectivity of Separation and the Determination of Anthocyanins of Fruits of Vaccinium Family Plants Using Acetonitrile–Formic Acid–Water Eluents. *Journal of Analytical Chemistry*, *75*(11), 1443-1450.

Eid, H. M., Ouchfoun, M., Brault, A., Vallerand, D., Musallam, L., Arnason, J. T., et al. (2014). Lingonberry (Vaccinium vitis-idaea L.) Exhibits Antidiabetic Activities in a Mouse Model of Diet-Induced Obesity. *Evidence-Based Complementary and Alternative Medicine, 2014*(1), 645812.

Fang, Q., Yu, L., Tian, F., Zhang, H., Chen, W., & Zhai, Q. (2023). Effects of dietary irritants on intestinal homeostasis and the intervention strategies. *Food Chemistry*, *409*, 135280.

Fu, J., Zong, X., Jin, M., Min, J., Wang, F., & Wang, Y. (2023). Mechanisms and regulation of defensins in host defense. *Signal Transduction and Targeted Therapy*, *8*(1), 300.

Fu, T., Coulter, S., Yoshihara, E., Oh, T. G., Fang, S., Cayabyab, F., et al. (2019). FXR regulates intestinal cancer stem cell proliferation. *Cell*, *176*(5), 1098-1112.

Guo, J., Chen, S., Zhang, Y., Liu, J., Jiang, L., Hu, L., et al. (2024). Cholesterol metabolism: physiological regulation and diseases. *MedComm*, *5*(2), e476.

He, Q., Zhang, Y., Ma, D., Zhang, W., & Zhang, H. (2022). Lactobacillus casei Zhang exerts anti-obesity effect to obese glut1 and gut-specific-glut1 knockout mice via gut microbiota modulation mediated different metagenomic pathways. *European journal of nutrition*, *61*(4), 2003-2014.

Heyman-Lindén, L., Kotowska, D., Sand, E., Bjursell, M., Plaza, M., Turner, C., et al. (2016). Lingonberries alter the gut microbiota and prevent low-grade

inflammation in high-fat diet fed mice. *Food & Nutrition Research*, *60*(1), 29993.

Hooper, L. V., Littman, D. R., & Macpherson, A. J. (2012). Interactions between the microbiota and the immune system. *Science*, *336*(6086), 1268-1273.

Huang, J., Liu, D., Wang, Y., Liu, L., Li, J., Yuan, J., et al. (2022). Ginseng polysaccharides alter the gut microbiota and kynurenine/tryptophan ratio, potentiating the antitumour effect of antiprogrammed cell death 1/programmed cell death ligand 1 (anti-PD-1/PD-L1) immunotherapy. *Gut*, *71*(4), 734-745.

Jamar, G., Estadella, D., & Pisani, L. P. (2017). Contribution of anthocyanin-rich foods in obesity control through gut microbiota interactions. *BioFactors*, *43*(4), 507-516.

Jeon, Y.-D., Lee, J.-H., Kang, S.-H., Myung, H., & Jin, J.-S. (2021). Lingonberry Fruit Ethanol Extract Ameliorates DSS-Induced Ulcerative Colitis In Vivo and In Vitro. *Applied Sciences*, *11*(17), 7955.

Kotowska, D., Neuhaus, M., Heyman-Lindén, L., Morén, B., Li, S., Kryvokhyzha, D., et al. (2022). Short-term lingonberry feeding is associated with decreased insulin levels and altered adipose tissue function in high-fat diet fed C57BL/6J mice. *Journal of Functional Foods*, *94*, 105125.

Kowalska, K. (2021). Lingonberry (Vaccinium vitis-idaea L.) Fruit as a Source of Bioactive Compounds with Health-Promoting Effects—A Review. *International Journal of Molecular Sciences*, *22*(10), 5126.

Kucera, C. R., Stranahan, L. W., Hughes, F., Blikslager, A. T., & Gonzalez, L. M. (2018). Protein biomarker of cell proliferation determines survival to discharge in cases of equine large colon volvulus. *Equine veterinary journal*, *50*(4), 452-456.

Li, S., Guo, J., Liu, R., Zhang, F., Wen, S. A., Liu, Y., et al. (2022). Predominance of Escherichia-Shigella in gut microbiome and its potential correlation with elevated level of plasma tumor necrosis factor alpha in patients with tuberculous meningitis. *Microbiology Spectrum*, *10*(6), e01926-22.

Li, W., Peregrina, K., Houston, M., & Augenlicht, L. H. (2020). Vitamin D and the nutritional environment in functions of intestinal stem cells: Implications for tumorigenesis and prevention. *The Journal of Steroid Biochemistry and Molecular Biology*, *198*, 105556.

Liu, Y., Fernandes, I., Mateus, N., Oliveira, H., & Han, F. (2024). The Role of Anthocyanins in Alleviating Intestinal Diseases: A Mini Review. Journal of Agricultural and Food Chemistry, 72(11), 5491-5502.

Liang, A., Leonard, W., Beasley, J. T., Fang, Z., Zhang, P., & Ranadheera, C. S. (2024). Anthocyanins-gut microbiota-health axis: A review. *Critical Reviews in Food Science and Nutrition*, *64*(21), 7563-7588.

Mattioli, R., Francioso, A., Mosca, L., & Silva, P. (2020). Anthocyanins: A comprehensive review of their chemical properties and health effects on cardiovascular and neurodegenerative diseases. *Molecules*, *25*(17), 3809.

Murai, T., & Matsuda, S. (2023). Fatty Acid Metabolites and the Tumor Microenvironment as Potent Regulators of Cancer Stem Cell Signaling. *Metabolites*, 13(6).

Mana, M. D., Hussey, A. M., Tzouanas, C. N., Imada, S., Barrera Millan, Y., Bahceci, D., et al. (2021). High-fat diet-activated fatty acid oxidation mediates intestinal stemness and tumorigenicity. *Cell Reports*, *35*(10).

Marungruang, N., Kovalenko, T., Osadchenko, I., Voss, U., Huang, F., Burleigh, S., et al. (2020). Lingonberries and their two separated fractions differently alter the gut microbiota, improve metabolic functions, reduce gut inflammatory properties, and improve brain function in ApoE−/− mice fed high-fat diet. *Nutritional Neuroscience*, *23*(8), 600-612.

Matziouridou, C., Marungruang, N., Nguyen, T. D., Nyman, M., & Fåk, F. (2016). Lingonberries reduce atherosclerosis in Apoe mice in association with altered gut microbiota composition and improved lipid profile. *Molecular Nutrition & Food Research*, *60*(5), 1150-1160.

Nateri, A. S., Spencer-Dene, B., & Behrens, A. (2005). Interaction of phosphorylated c-Jun with TCF4 regulates intestinal cancer development. *Nature*, *437*(7056), 281-285.

Nguyen, N. T., Sun, W.-H., Chen, T.-H., Tsai, P.-C., Chen, C.-C., & Huang, S.-L. (2022). Gut Mucosal Microbiome Is Perturbed in Rheumatoid Arthritis Mice and Partly Restored after TDAG8 Deficiency or Suppression by Salicylanilide Derivative. *International Journal of Molecular Sciences*, *23*(7), 3527.

Pärnänen, P., Lähteenmäki, H., Tervahartiala, T., Räisänen, I. T., & Sorsa, T. (2021). Lingonberries—General and Oral Effects on the Microbiome and Inflammation. *Nutrients*, *13*(11), 3738.

Ryyti, R., Hämäläinen, M., Peltola, R., & Moilanen, E. (2020). Beneficial effects of lingonberry (Vaccinium vitis-idaea L.) supplementation on metabolic and inflammatory adverse effects induced by high-fat diet in a mouse model of obesity. *PLOS ONE*, *15*(5), e0232605.

Ryyti, R., Hämäläinen, M., Tolonen, T., Mäki, M., Jaakkola, M., Peltola, R., et al. (2024). Lingonberry (Vaccinium vitis-idea L.) Skin Extract Prevents Weight Gain and Hyperglycemia in High-Fat Diet-Induced Model of Obesity in Mice. *Nutrients*, *16*(13), 2107.

Slabá, H., Määttänen, M., Marttinen, M., Lapinkero, V., Päivärinta, E., & Pajari, A.-M. (2023). Daily berry consumption attenuates β-catenin signalling and genotoxicity in colon carcinoma cells exposed to faecal water from healthy volunteers in a clinical trial. *Journal of Functional Foods*, *102*, 105440.

Su, Q., Huang, J., Chen, X., Wang, Y., Shao, M., Yan, H., et al. (2023). Long-Term High-Fat Diet Decreases Renal Insulin-Degrading Enzyme Expression and Function by Inhibiting the PPARγ Pathway. *Molecular Nutrition & Food Research*, *67*(7), 2200589.

Turdo, A., Porcelli, G., D'Accardo, C., Di Franco, S., Verona, F., Forte, S., et al. (2020). Metabolic escape routes of cancer stem cells and therapeutic opportunities. *Cancers*, *12*(6), 1436.

Vernia, F., Longo, S., Stefanelli, G., Viscido, A., & Latella, G. (2021). Dietary factors modulating colorectal carcinogenesis. *Nutrients*, *13*(1), 143.

Wang, M., Luan, X., Yan, Y., Zheng, Q., Chen, W., & Fang, J. (2021). Wnt6 regulates

the homeostasis of the stem cell niche via Rac1-and Cdc42-mediated noncanonical Wnt signalling pathways in Drosophila testis. *Experimental Cell Research*, *402*(1), 112511.

Wu, F., Lei, H., Chen, G., Chen, C., Song, Y., Cao, Z., et al. (2022). Multiomics analyses reveal that long-term intake of hesperetin-7-O-glucoside modulates the gut microbiota and bile acid metabolism in mice. *Journal of Agricultural and Food Chemistry*, *70*(47), 14831-14840.

Xie, Y., Ding, F., Di, W., Lv, Y., Xia, F., Sheng, Y., et al. (2020). Impact of a high-fat diet on intestinal stem cells and epithelial barrier function in middle-aged female mice. *Molecular Medicine Reports*, *21*(3), 1133-1144.

Yan, C., Huang, S. H., Ding, H. F., Kwek, E., Liu, J. H., Chen, Z. X., et al. (2023). Adverse effect of oxidized cholesterol exposure on colitis is mediated by modulation of gut microbiota. *Journal of Hazardous Materials*, *459*, 132057.

Yao, C., Gou, X., Tian, C., Zhou, L., Hao, R., Wan, L., et al. (2023). Key regulators of intestinal stem cells: diet, microbiota, and microbial metabolites. *Journal of Genetics and Genomics*, *50*(10), 735-746.

Zafar, H., & Saier Jr, M. H. (2021). Gut Bacteroides species in health and disease. *Gut Microbes*, *13*(1), 1848158.

Zhao, C., Bao, L., Qiu, M., Wu, K., Zhao, Y., Feng, L., et al. (2022). Commensal cow Roseburia reduces gut-dysbiosis-induced mastitis through inhibiting bacterial translocation by producing butyrate in mice. *Cell Reports*, *41*(8).

Zhou, X., Zhang, D., Qi, W., Hong, T., Xiong, T., Wu, T., et al. (2021). Exopolysaccharides from Lactobacillus plantarum NCU116 facilitate intestinal homeostasis by modulating intestinal epithelial regeneration and microbiota. *Journal of Agricultural and Food Chemistry*, *69*(28), 7863-7873.

Zhu, L., Zhang, Y., Li, Y., Wang, H., Shen, G., & Wang, Z. (2022). Inhibitory effect of lingonberry extract on HepG2 cell proliferation, apoptosis, migration, and invasion. *PLOS ONE*, *17*(7), e0270677.

Zhu, H., Gu, B., Zhao, D., Ma, Y., Mehmood, M. A., Li, Y., et al. (2024). Wuliangye strong aroma baijiu promotes intestinal homeostasis by improving gut microbiota and regulating intestinal stem cell proliferation and differentiation. *Journal of the Science of Food and Agriculture*, *104*(12), 7417-7428.

Zhu, J., Wang, Y., Wang, W., Wu, B., Lu, Y., Du, J., et al. (2022). Mptx2 defends against peritoneal infection by methicillin-resistant staphylococcus aureus. *International Immunopharmacology*, *108*, 108856.

632 **Table 1 Quantities of anthocyanins in ARLE**

Peak	Composition	Retention Time (min)	Content (mg/g)
1	Delphinidin-3-O-glucoside chloride	11.897	48.0±0.3
2	Delphinidin-3-O-arabinoside chloride	14.157	40.8±0.3
3	Cyanidin-3-O-galactoside chloride	16.170	32.8±0.2
4	Delphinidin-3-O-galactoside chloride	16.823	40.6±0.3
5	Cyanidin-3-O-glucoside chloride	19.103	40.2±0.3
6	Peonidin-3-O-glucoside chloride	20.533	15.7±0.07
7	Cyanidin-3-O-arabinoside chloride	21.257	27.8±0.1
8	Petunidin 3-O-glucoside chloride	23.353	32.5±0.2
9	Delphinidin chloride	24.633	1.8±0.02
10	Peonidin-3-O-galactoside chloride	25.463	4.1±0.03
11	Petunidin-3-O-arabinoside chloride	25.983	10.5±0.04
12	Petunidin-3-O-glucoside chloride	28.843	15.4±0.1
13	Malvidin-3-O-galactoside chloride	29.353	11.2±0.04
14	Peonidin-3-O-arabinoside chloride	31.167	2.1±0.04
15	Malvidin-3-O-glucoside chloride	32.327	26.0±0.05
16	Cyanidin chloride	34.234	2.1±0.03
17	Malvidin-3-O- arabinoside chloride	35.123	6.7±0.18
18	Petunidin chloride	39.083	0.9±0.02
19	Peonidin chloride	43.167	0.3±0.01
20	Malvidin chloride	43.623	0.9±0.02

633 **Figure legends**

634 **Fig. 1 HPLC analysis of anthocyanin profile in ARLE at 535 nm.** (A)
635 Chromatogram of mixed standards. (B) Chromatogram of ARLE.

636 **Fig. 2 ARLE mitigated the negative physiological effects on HFD-fed mice.** (A)
637 Experimental design for the mice fed the HFD. (B) Body diagram of the mice. (C) Body
638 weight curve. (D) Body weight gain. (E) Food intake. (F) Calorie intake. (G) Lee's
639 index. (H) Adipose tissue index. (I) Triglyceride (TG). (J) Total cholesterol (TC), (K)
640 Low-density lipoprotein (LDL-C). (L) High-density lipoprotein (HDL-C). The data are
641 expressed as the means±SEMs (n=10). One-way analysis of variance (ANOVA) with
642 Tukey's test was used for multiple comparisons. $*P< 0.05$, $**P< 0.01$.

643 **Fig. 3 ARLE improved the intestinal homeostasis of HFD-fed mice.** (A-a, b, c) H&E
644 staining of mouse jejunum pathology. (B-a, c, e) H&E staining of the colon. (B-b, d, f)
645 PAS staining of the colon. (C-a, d, g) MUC2 immunofluorescence staining of the
646 jejunum; (C-b, e, h) Immunofluorescence staining image of the MUC2 protein; (C-c, f,
647 i) Enlarged MUC2 images of immunofluorescence staining. (D) Jejunal villus length.
648 (E) The depth of the jejunum crypts. (F) Colon wall thickness. (G) The percentage of
649 PAS-positive area in the colonic crypt. (H) Colon goblet cell count. (I) Fluorescence
650 intensity of the MUC2 protein. (J) Expression level of the *MUC2* gene. (K) Relative
651 expression of MUC2 protein. One-way analysis of variance (ANOVA) with Tukey's
652 test was used for multiple comparisons.$*P< 0.05$, $**P< 0.01$.

653 **Fig. 4 ARLE controlled the malignant proliferation and differentiation of ISCs in**
654 **HFD-fed mice.** (A-a, b, c) Immunohistochemistry image of PNCA in the jejunum; (A-

d, e, f) enlarged immunohistochemistry image of PNCA. (B-a, d, g) Immunofluorescence and DAPI staining image of Lgr5 protein in the jejunum; (B-b, e, h) Immunofluorescence staining image of Lgr5 protein; (B-c, f, i) Enlarged images of Lgr5 immunofluorescence staining. (C-a, d, g) Immunofluorescence and DAPI staining image of the Ki67 protein in the jejunum; (C-b, e, h) Immunofluorescence staining image of the Ki67 protein; (C-c, f, i) Enlarged Ki67 images of immunofluorescence staining. (D-a, d, g) Immunofluorescence and DAPI staining images of the SOX9 protein in the jejunum. (D-b, e, h) Immunofluorescence staining image of the SOX9 protein. (D-c, f, i) Enlarged SOX9 immunofluorescence images. (E) Percentage of PCNA-positive area. (F) Expression level of the *PCNA* gene. (G) Fluorescence intensity of the Ki67 protein. (H) Expression level of the *Ki67* gene. (I) Fluorescence intensity of the Lgr5 protein. (J) Expression level of the *Lgr5* gene. (K) Fluorescence intensity of the SOX9 protein. (L) Expression level of the *SOX9* gene. (M-P) Western blot analysis of Ki67, Lgr5, and SOX9 protein expression. One-way analysis of variance (ANOVA) with Tukey's test was used for multiple comparisons. **P*< 0.05, ***P*< 0.01.

Fig. 5 ARLE regulated the intestinal microflora of HFD-fed mice. (A) Observed_species. (B) Shannon. (C) ACE. (D) Chao1. (E) The F/B ratio. (F) PCoA analysis. (G) NMDS analysis. (H) Family-level microbial abundance. (I) Genus-level microbial abundance. (J) Horizontal clustering heatmap. (K-S) Bacterial abundance at the genus level. The asterisk in Fig. A-E indicated the significant difference according

676 to Tukey's multiple comparisons. The asterisk in Fig. K-S indicated the significant
677 difference according to the T-test. *P< 0.05, **P< 0.01.

678 **Fig. 6 ARLE manipulated the expression of genes related to the immune response**
679 **in the intestine of HFD-fed mice.** (A) Principal component analysis of the mouse
680 intestinal gene expression profile. (B) Volcano plot of differentially expressed genes.
681 (D) GO pathway enrichment differential expression annotation. (C, D) GSEA of the
682 innate immune response in the mucosa. (E, F) GSEA of *Staphylococcus aureus*-infected
683 cells. (G) Combined analysis of the microbiome and transcriptome. The asterisk
684 indicated the significant difference according to the T-test. *P< 0.05, **P< 0.01.

685 **Fig. 7 ARLE affected the signaling pathways involved in ISCs calibration in the**
686 **intestine of HFD-fed mice**. (A) GSEA of the PPAR signaling pathway. (B) GSEA of
687 the Wnt signaling pathway. (C) Western blot image of the c-Jun, Rac1, Wnt6 and
688 PPARd proteins. (D) c-Jun protein content in the jejunum. (E) Rac1 protein content in
689 the jejunum. (F) PPARd protein content in the jejunum. (G) Wnt6 protein content in the
690 jejunum. (H) *c-Jun* gene expression levels. (I) *Rac1* gene expression levels. (J) *PPARd*
691 gene expression levels. (K) *Wnt6* gene expression levels. The asterisk indicated the
692 significant difference according to Tukey's multiple comparisons. *P< 0.05, **P< 0.01.
693
694
695
696
697

Fig. 1

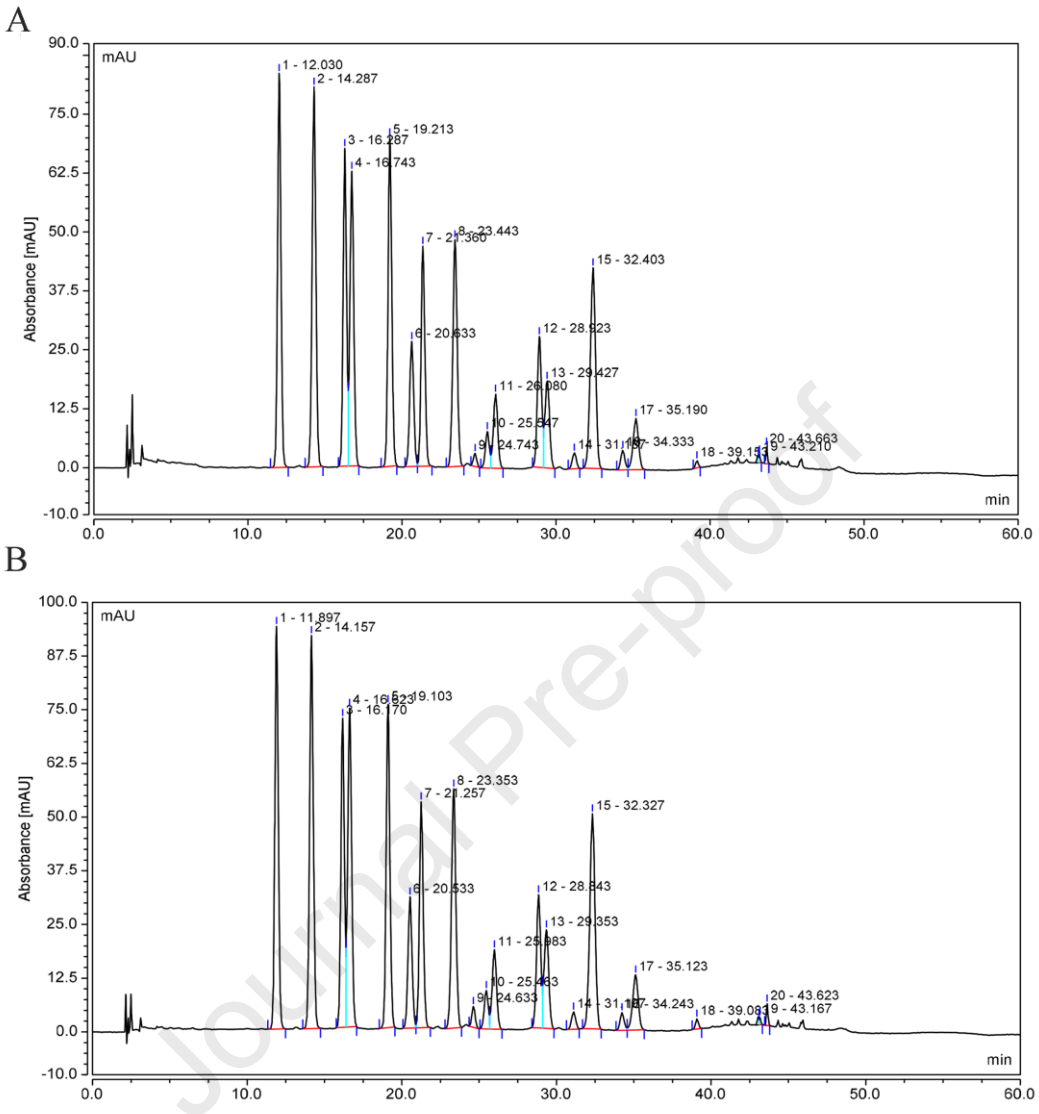

Fig. 2

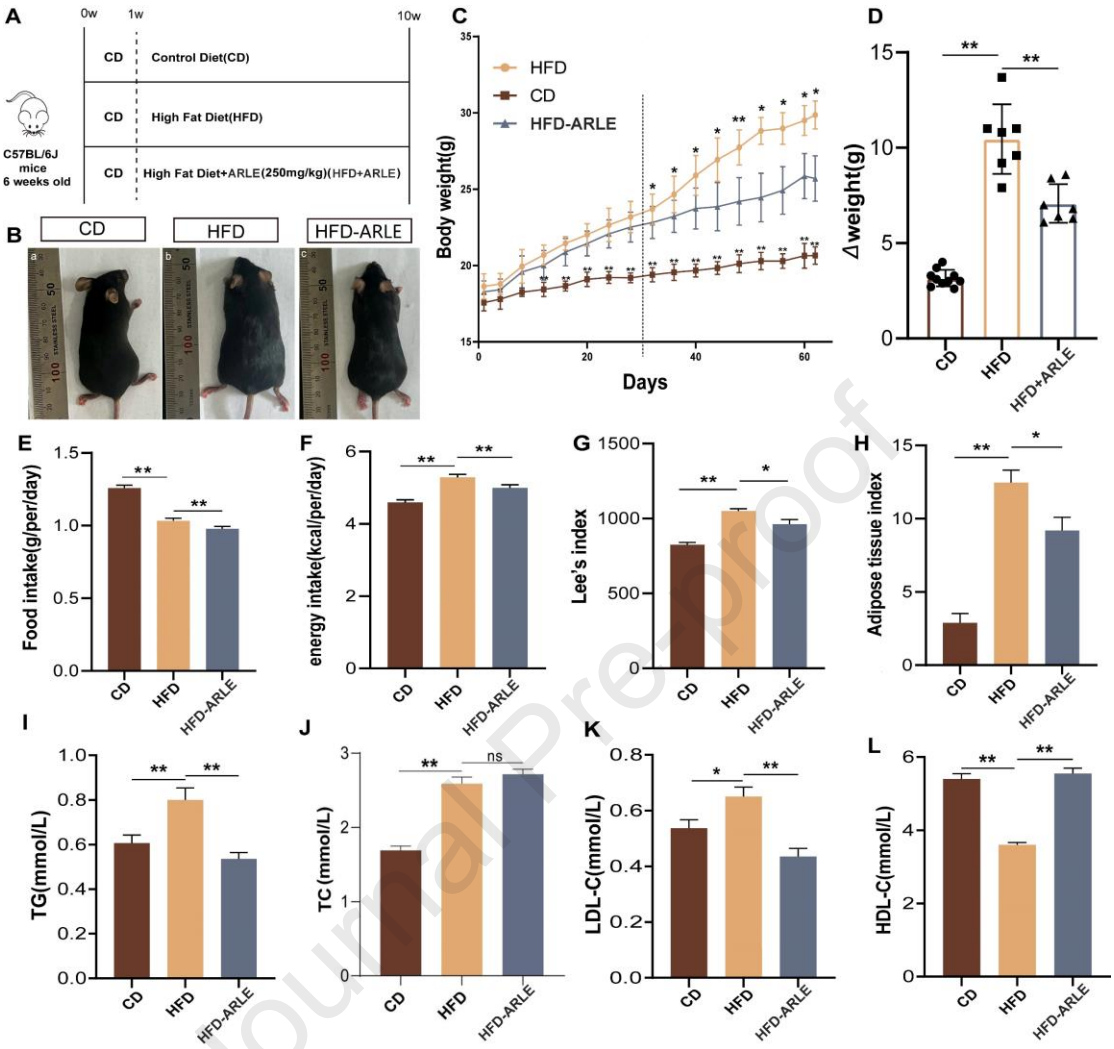

718 **Fig. 3**

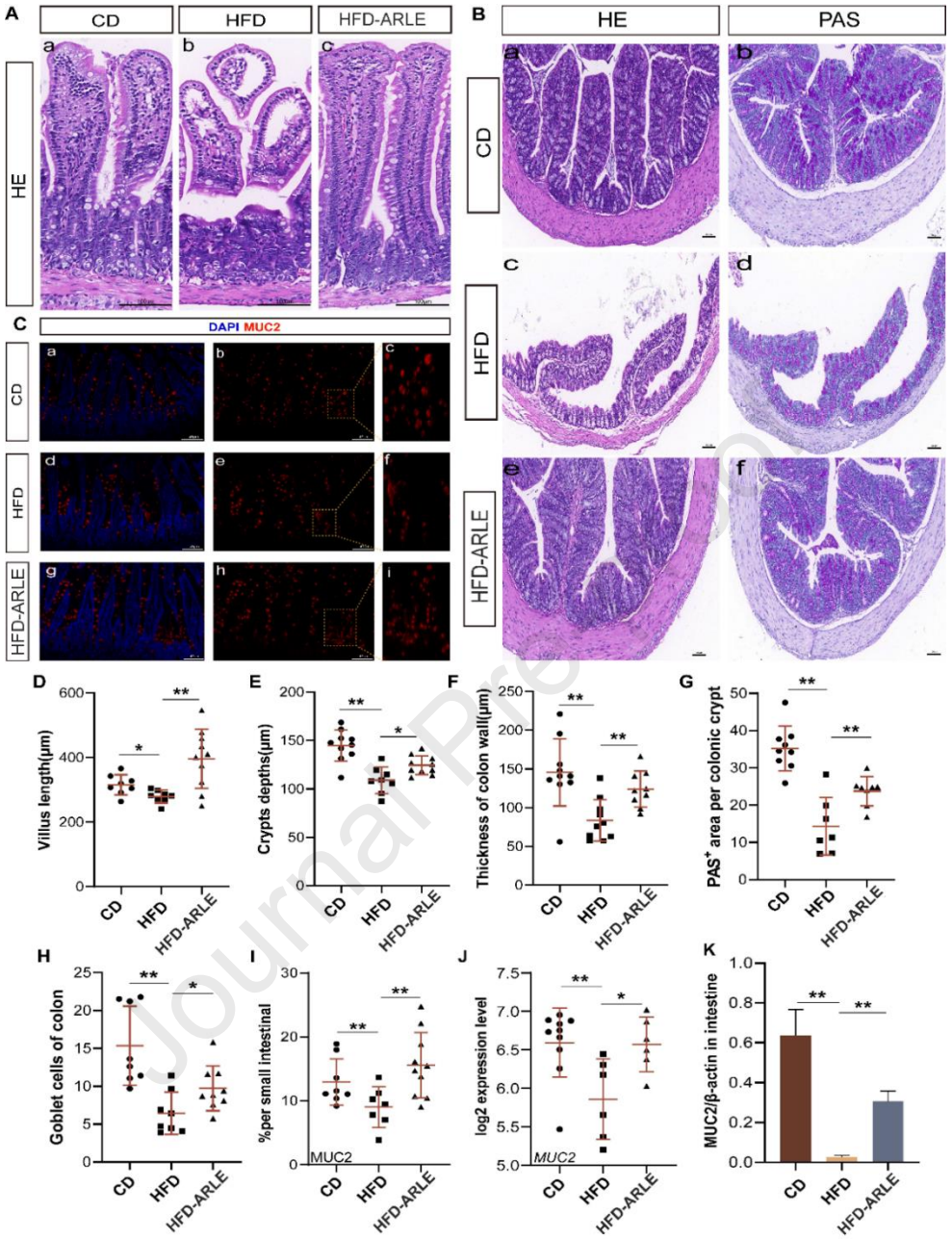

719

720

721

722

723

724

725

Fig. 4

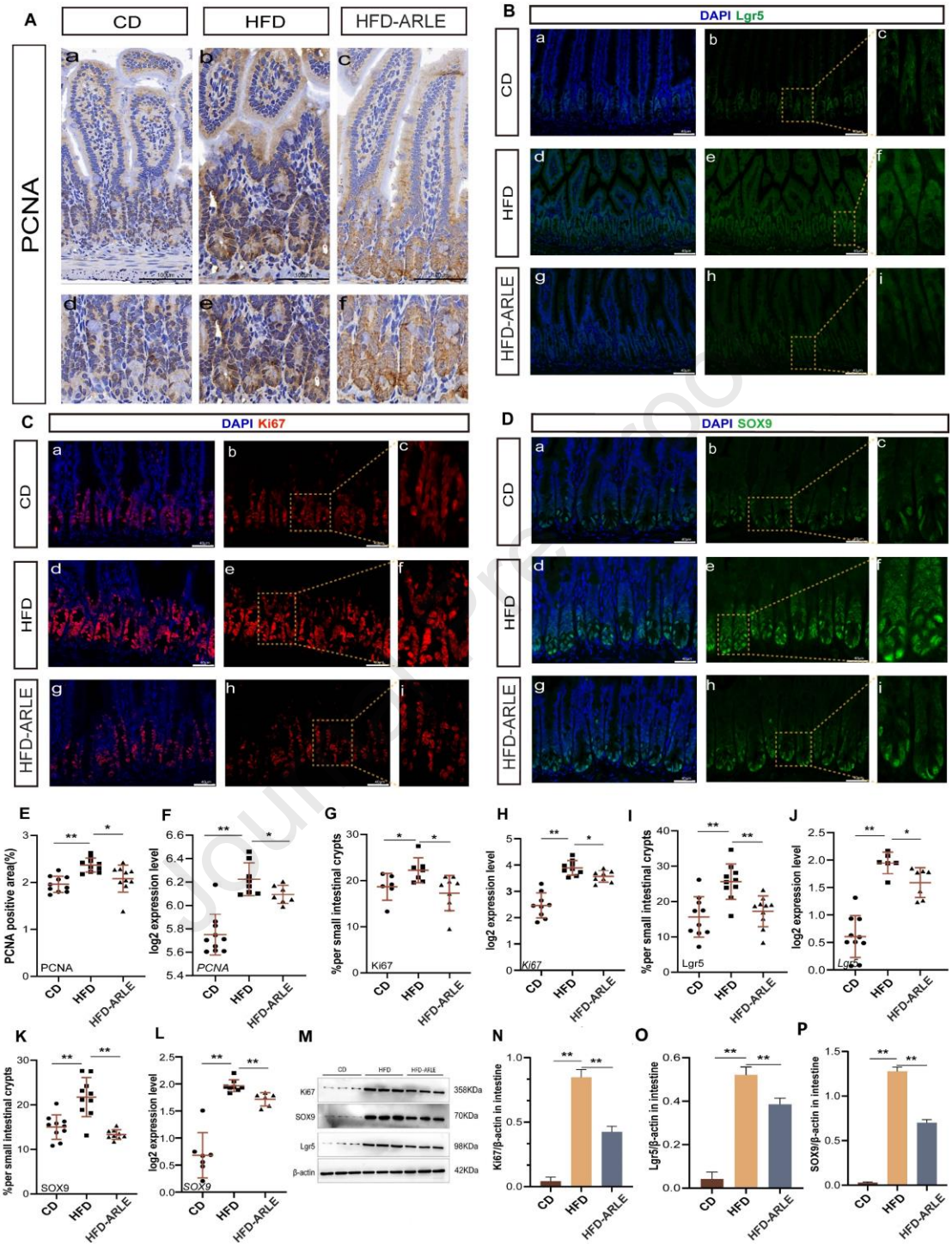
A
CD
HFD
HFD-ARLE
PCNA
B
DAPI Lgr5
C
DAPI Ki67
D
DAPI SOX9
E
PCNA positive area(%)
F
log2 expression level
G
%per small intestinal crypts
H
log2 expression level
I
%per small intestinal crypts
J
log2 expression level
K
%per small intestinal crypts
L
log2 expression level
M
Ki67
SOX9
Lgr5
β-actin
358KDa
70KDa
98KDa
42KDa
N
Ki67/β-actin in intestine
O
Lgr5/β-actin in intestine
P
SOX9/β-actin in intestine

731 **Fig. 5**

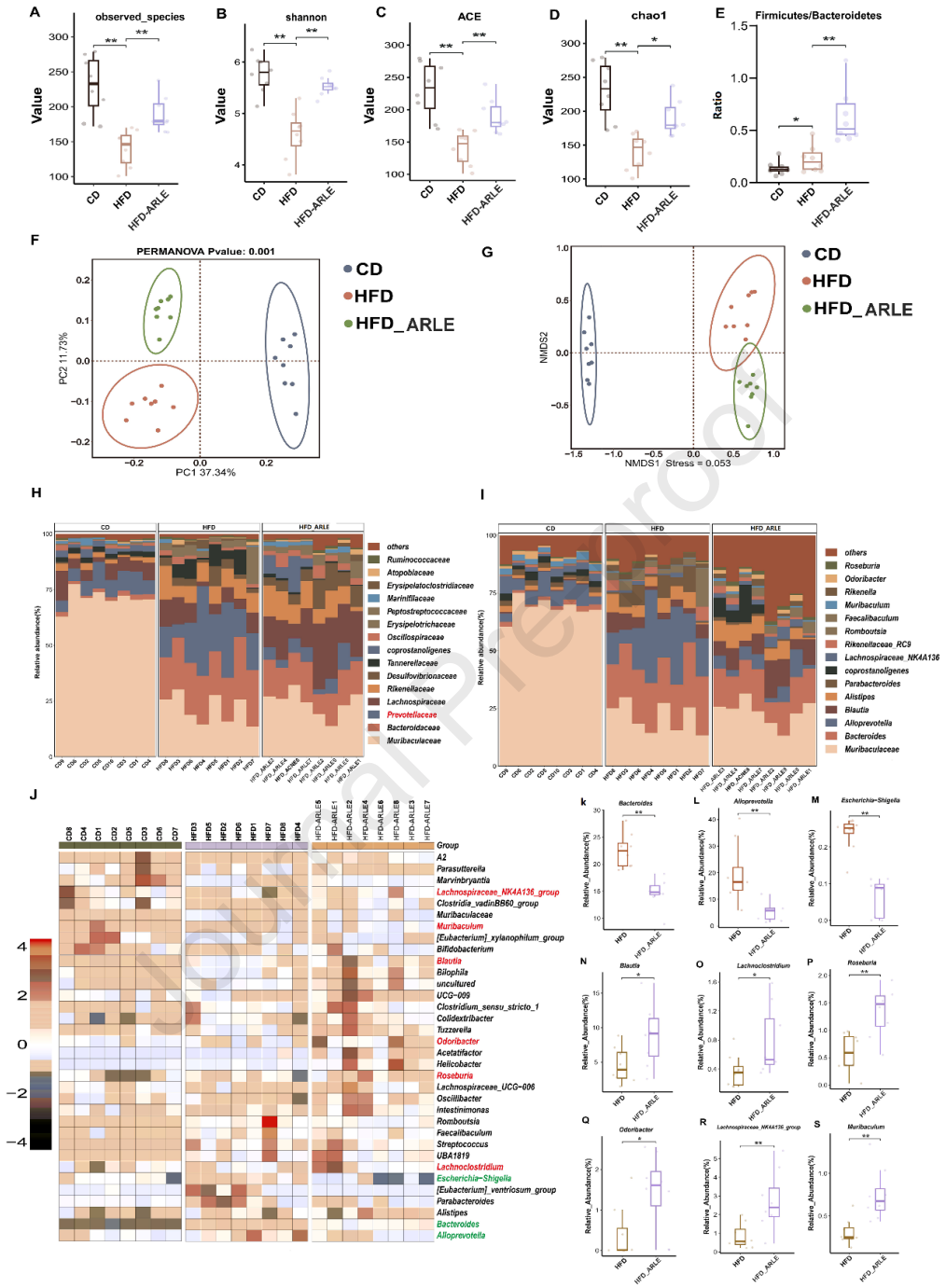

732

733

734

735

736

737 **Fig. 6**

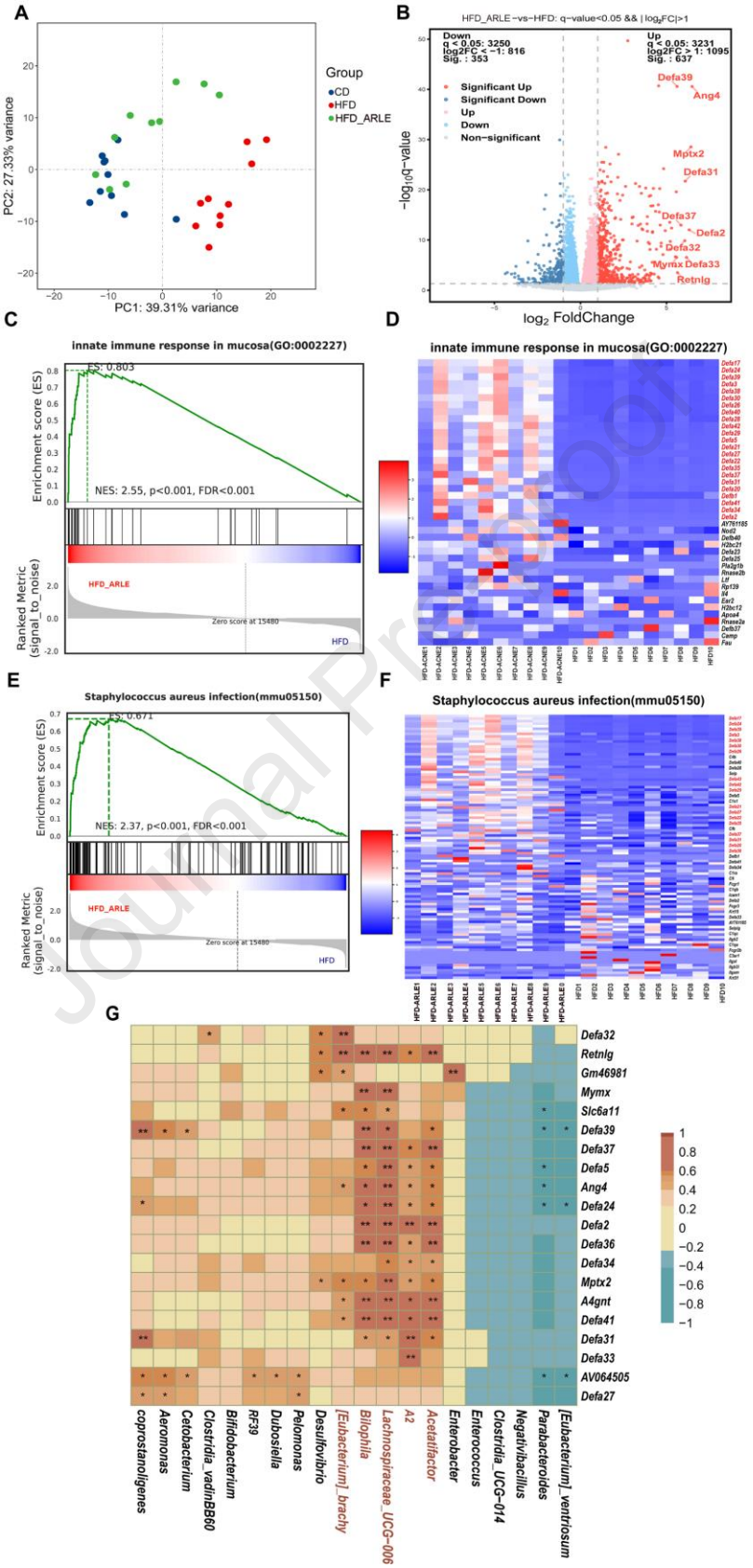

738

739

Fig. 7

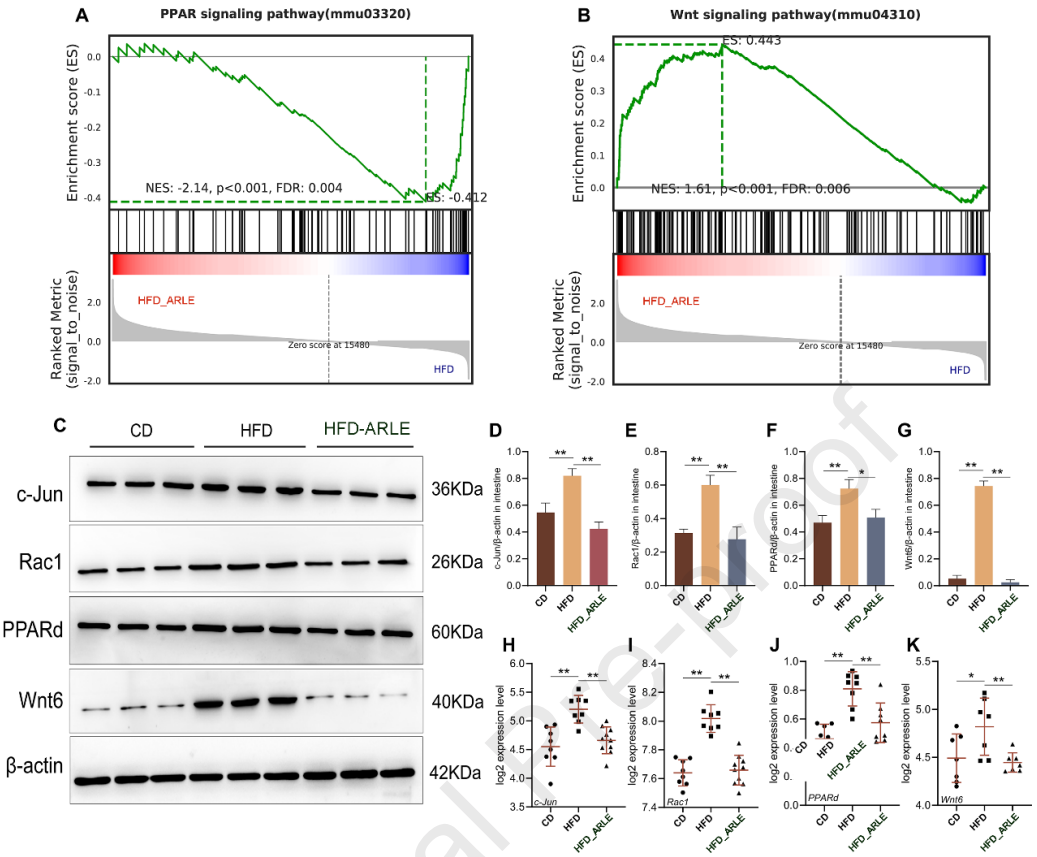
A
PPAR signaling pathway(mmu03320)
Enrichment score (ES)
NES: -2.14, p<0.001, FDR: 0.004
ES: -0.412
Ranked Metric (signal_to_noise)
HFD_ARLE
Zero score at 15480
HFD
B
Wnt signaling pathway(mmu04310)
ES: 0.443
NES: 1.61, p<0.001, FDR: 0.006
C
CD
HFD
HFD-ARLE
c-Jun
Rac1
PPARd
Wnt6
β-actin
36KDa
26KDa
60KDa
40KDa
42KDa
D
E
F
G
H
I
J
K
log2 expression level

Highlights

1. ARLE reduces the weight gain and dyslipidemia of HFD-induced mice.
2. ARLE maintains the intestinal health of HFD-induced mice by modulating gut microbiota.
3. ARLE balances the proliferation and differentiation of ISCs with improving immune capability.
4. ARLE improves intestinal homeostasis by regulating Wnt/PPAR-mediated ISCs.

Declaration of interests

☒ The authors declare that they have no known competing financial interests or personal relationships that could have appeared to influence the work reported in this paper.

☐The authors declare the following financial interests/personal relationships which may be considered as potential competing interests: